Investigating the bulge morphology of dual AGN host galaxies from the GOTHIC survey

C. P. Nehal,[1]★ Mousumi Das [ORCID],[2]★ Sudhanshu Barway [ORCID],[2] Francoise Combes [ORCID],[3] Prerana Biswas [ORCID],[2] Anwesh Bhattacharya[4] and Snehanshu Saha [ORCID][4,5]

[1]*Department of Physics, Indian Institute of Science Education and Research, Bhopal 462066, India*
[2]*Indian Institute of Astrophysics, Bangalore 560034, India*
[3]*Observatoire de Paris, LERMA, College 'de France, PSL University, Sorbonne University, CNRS, F-75014 Paris, France*
[4]*Siebel School of Computing and Data Science, University of Illinois at Urbana-Champaign, Urbana, IL 61801, USA*
[5]*5APPCAIR, Department of CSIS, Birla Institute of Technology & Science and HappyMonk AI, Goa 403726, India*

ABSTRACT

We present a structural analysis of bulges in dual active galactic nuclei (AGNs) host galaxies. Dual AGNs arise in galaxy mergers where both supermassive black holes are actively accreting. The AGNs are typically embedded in compact bulges, which appear as luminous nuclei in optical images. Galaxy mergers can result in bulge growth, often via star formation. The bulges can be discy (pseudo-bulges), classical bulges, or belong to elliptical galaxies. Using Sloan Digital Sky Survey Data Release 18 *gri* images and GALFIT modelling, we performed 2D decomposition for 131 dual AGNs bulges (comprising 61 galaxy pairs and 3 galaxy triplets) identified in the GOTHIC survey. We derived Sérsic indices, luminosities, masses, and scale lengths of the bulges. Most bulges (105/131) are classical, with Sérsic indices lying between $n = 2$ and $n = 8$. Among these, 64 per cent are elliptical galaxies, while the remainder are classical bulges in disc galaxies. Only $\sim$20 per cent of the sample exhibits pseudo-bulges. Bulge masses span $1.5 \times 10^9 \, M_\odot$ to $1.4 \times 10^{12} \, M_\odot$, with the most massive systems being ellipticals. Galaxy-type matching shows that elliptical–elliptical and elliptical–disc mergers dominate over disc–disc mergers. At least one galaxy in two-thirds of the dual AGN systems is elliptical and only $\sim$30 per cent involve two disc galaxies. Although our sample is limited, our results suggest that dual AGNs preferentially occur in evolved, red, quenched systems, which typically form via major mergers. They are predominantly hosted in classical bulges or elliptical galaxies rather than star-forming disc galaxies.

Key words: galaxies: active – galaxies: bulges – galaxies: evolution – galaxies: interactions – galaxies: nuclei – galaxies: structure.

1 INTRODUCTION

Galaxy mergers are important for the hierarchical growth of galaxies and the formation of structure in our Universe (S. D. White & C. S. Frenk 1991). As the merging galaxies come closer, the gravitational torques generated by their interaction affect their stellar and gas distributions, resulting in increased star formation and the growth of stellar mass (P. F. Hopkins et al. 2009, 2010). Studies show that gas-rich major mergers or wet mergers can have star formation rates (SFRs) that are $\sim$100 times that before the interaction. Such enhanced SFRs are often found in starburst galaxies or ultraluminous infrared galaxies (ULIRGs; J. C. Mihos & L. Hernquist 1996; T. J. Cox et al. 2004; F. Li et al. 2025). The merger-induced SFR is the highest for similar galaxy mass ratios, as observed in ULIRGs (S. Nandi, M. Das & K. S. Dwarakanath 2021), and drops rapidly with increasing galaxy mass ratios (T. J. Cox et al. 2008). If the galaxies are gas-poor, then there is little or no associated star formation, and the merger is called a dry merger. The ensuing bulge or central spheroidal growth

in the merger remnant arises from merger-accreted stars from the companion galaxies (L. Quilley & V. de Lapparent 2022), especially in the case of minor mergers (J. Zavala et al. 2012).

The enhanced nuclear gas inflow and star formation activity can trigger mass accretion onto the supermassive black holes (SMBHs), in which case the nuclei become active galactic nuclei (AGNs; A. L. Schechter et al. 2025). When both nuclear SMBHs start accreting mass, they will form an AGN pair, or in other words, a dual AGN (K. Rubinur, M. Das & P. Kharb 2019; K. Rubinur et al. 2021). Although the initial detection of dual AGN was serendipitous (S. Komossa et al. 2003), recent surveys have found large samples of dual AGN (Y.-W. Zhang et al. 2021; A. Bhattacharya et al. 2023). A few triple AGNs have also been detected (R. W. Pfeifle et al. 2019; J. Yadav et al. 2021; S. Keshri et al. 2025). However, dual AGNs are still rare and triple AGNs are even rarer. In the literature, dual AGNs are generally defined as close mergers with AGN separations $\sim$1– 40 kpc, whereas binary AGNs have nuclei separations <100 pc (e.g. K. Rubinur, M. Das & P. Kharb 2018; A. De Rosa et al. 2019). Since galaxy mergers are often associated with star formation, the nature of nuclei in close mergers can have different combinations, such as

★ E-mail: ncp.sudo@gmail.com (CPN); mousumi@iiap.res.in (MD)

star-forming pairs (SF–SF), mixed pairs (SF–AGN), or dual AGN (A. Bhattacharya et al. 2023). Since the discovery of gravitational waves from merging black holes (B. P. Abbott et al. 2016), there has been a growing interest in detecting and studying dual and binary AGNs (P. Kharb, D. V. Lal & D. Merritt 2017; M. Bailes et al. 2021; S. Mondal et al. 2024). This is because inspiralling SMBHs at separations <1 pc will give rise to nHz and mHz gravitational waves (S. Burke-Spolaor et al. 2019), and so AGN pairs are a means to study the formation of binary SMBHs (H. Padmanabhan & A. Loeb 2024). A good example of a binary SMBH system in a very late stage of merging is OJ 287, but very little is known about its host galaxy (M. J. Valtonen et al. 2022, 2025).

During mergers, as the individual SMBHs spiral towards the centre of mass, they will still be surrounded by a significant number of closely bound stars and thus be embedded in compact bulges or spheroids. In optical or X-ray images, these bulges will appear as bright nuclei (M. Das et al. 2018), and some may host dual AGN, depending on the SMBH accretion rates (M. Koss et al. 2012; G. Giri et al. 2022). Although dual AGN properties have been extensively studied using multiwavelength observations, not much is known about their host bulges. Are they all classical bulges that are spherical in shape, or do they have oval or boxy morphology? For example, if the host galaxies are disc galaxies, the SMBHs may be embedded in bulges that are more discy, since their stellar mass may have grown via gas accreted along the galaxy plane during mergers (J. Zavala et al. 2012). Alternatively, the bulges may be boxy or peanut-shaped if they evolved from bar instabilities or disc thickening (S. Ghosh et al. 2024). It is also possible that they have grown through a combination of both processes (J. Méndez-Abreu et al. 2014); both processes are part of the secular evolution of galaxy discs (J. Kormendy & R. C. Kennicutt 2004).

In dry mergers, the merging galaxies are usually elliptical or lenticular, and the SMBHs will be embedded in extended spheroidal bulges. So understanding the bulge–disc morphology of large samples of merging galaxies can reveal the nature of the merging galaxies as well as predict the possible outcome of the merger, i.e. is an elliptical merging pair or a disc galaxy pair more likely to form a dual AGN? Or are dual AGN more likely to be found in mixed disc–elliptical merging pairs? Also important is that AGNs are known to evolve with their bulges, and their coevolution leads to the well-known correlation between the nuclear velocity dispersion (or bulge luminosities), with SMBH mass (M–σ relation; C. Marsden et al. 2020). Hence, deriving bulge morphologies in dual AGN is another way of understanding AGN–bulge coevolution in different environments. Finally, bulge evolution in merging galaxies is an important part of the larger picture of galaxy evolution. Thus, there are a plethora of reasons for understanding the nature of bulges in dual AGN as well as in merging galaxies.

Bulges are broadly of two types, classical bulges and pseudo-bulges (D. B. Fisher & N. Drory 2016). Classical bulges are dispersion-dominated stellar systems and appear as compact, bright spheroids in galaxy centres, whereas pseudo-bulges have a relatively stronger disc component and appear as oval or boxy in shape (V. P. Debattista et al. 2004; A. Kumar, M. Das & S. K. Kataria 2021). Classical bulges are formed in early epochs due to the monolithic collapse of gas clouds, and continue to grow through mergers (O. J. Eggen, D. Lynden-Bell & A. R. Sandage 1962; A. Brooks & C. Christensen 2016), whereas pseudo-bulges are formed via secular evolution of galaxy discs (J. Kormendy & D. B. Fisher 2008). Bulges can be quantitatively analysed using the Sérsic index value n (A. W. Graham & S. P. Driver 2005). Pseudo-bulges have a Sérsic index value $n < 2$, while classical bulges have values $n > 2$ (D. A. Gadotti

2009). Studies show that bulges are closely related to their host galaxies; the discs of pseudo-bulge host galaxies are younger and have more star formation compared to the discs associated with classical bulges (K. Vaghmare, S. Barway & A. Kembhavi 2013; J. Hu et al. 2024a). Also, the fraction of pseudo-bulges increase at lower redshifts as the bulge to disc fraction evolves with time (A. Kumar & S. K. Kataria 2022). In general the effect of mergers on bulges also depends on redshifts, as merger rates were higher at early epochs (C. R. Bridge, R. G. Carlberg & M. Sullivan 2010; S. Sachdeva, K. Saha & H. P. Singh 2017).

In this paper, we focus on deriving the bulges and host galaxy types of dual AGN. Our main aims are the following. (i) Determine the Sérsic indices of the dual AGN bulges using the bulge–disc decomposition program GALFIT. (ii) Hence, determine the nature of the host galaxies of the dual AGN. (iii) Derive bulge masses and bulge mass ratios. (iv) Determine whether dual AGNs are more likely to be found in elliptical galaxy pairs, disc galaxy pairs, or mixed elliptical–disc pairs. This is an important question as it addresses the probability of finding SMBH pairs in early-type galaxies or disc galaxies. The paper is organized as follows. Section 2 describes the sample and outlines the two-dimensional decomposition of the galaxies. Section 3 presents the results of the decomposition. Section 4 discusses these results. A summary is provided in Section 5. Throughout this paper, a flat ΛCDM (Λ cold dark matter) cosmology is used with $H_0 = 70\,\mathrm{km\,s^{-1}\,Mpc^{-1}}$, $\Omega_m = 0.3$, and $\Omega_\Lambda = 1 - \Omega_m$.

2 SAMPLE AND ANALYSIS

2.1 GOTHIC sample

Our sample is drawn from our previous study of galaxy mergers, where we detected pairs of galaxy nuclei in an automated way using a novel algorithm called GOTHIC (A. Bhattacharya et al. 2023). After applying the algorithm to a sample of one million galaxies derived from Sloan Digital Sky Survey (SDSS) Data Release 16, we obtained a confirmed sample of 681 close nuclei pairs. Furthermore, to classify the type of nuclear activity in the host galaxy nuclei, we applied the AGN diagnostic plot of Baldwin–Phillips–Telverich (BPT; J. A. Baldwin, M. M. Phillips & R. Terlevich 1981). Using the BPT plot, we derived a sample of 159 dual AGNs, which also included two triplets and one quadruplet system of galaxies. We used this sample of dual AGN in this study. The systems in this study are examples of binary galaxies that have evolved further into very close merging systems. How nuclear activity arises in the early stages of separate pairs of galaxies should have a bearing on the activity when the merger has happened, as discussed in G. Byrd & M. Valtonen (2001).

2.2 2D image decomposition of galaxies

Bulge–disc decomposition was carried out using the GALFIT software package (C. Y. Peng et al. 2002) to investigate bulge properties in a sample of dual AGN. Imaging data were retrieved from SDSS Data Release 18 (DR18), which provides calibrated FITS images for the target galaxies. A 200×200 pixels cut-out centred on one nucleus was extracted for each system. As the FITS images are in units of nanomaggies (NMGY) per pixel, a conversion to counts per pixel, required by GALFIT, was applied using the NMGY scaling factor provided in the FITS headers. Although SDSS DR18 provides sky-subtracted images with near-zero background levels, GALFIT requires a non-zero sky value for numerical stability. To satisfy this condition, a constant offset of 1000 counts was added to all pixels,

and the same value was specified as the sky level in the GALFIT input. This modification significantly improved the convergence and robustness of the fitting procedure. A point spread function (PSF) image was constructed from a nearby unsaturated star in the same field and provided to GALFIT to account for PSF convolution during the modelling process. Foreground stars and background sources occasionally introduced poor fits and inflated reduced chi-squared (χ_ν^2) values. Mask images were created to exclude these objects and were incorporated into the GALFIT input via the feedme files. Galaxies with angular sizes comparable to the PSF were excluded to ensure reliable structural measurements. A minimum size criterion of twice the PSF full width at half-maximum (FWHM) was adopted, resulting in a refined sample of 104 dual AGN systems from an initial set of 159.

Initial parameter estimates for all the sample galaxies were obtained from the SDSS 'photoObj' catalogue. To ensure reliable structural fitting, the FWHM of PSF (PSF-FWHM) was compared with the de Vaucouleurs radius (deVRad) in each of the five bands. Galaxies with deVRad $< 2 \times$ PSF-FWHM were excluded from the analysis. After applying this criterion, a final sample of 104 merging galaxies was selected for GALFIT modelling.

Estimation of initial parameters, such as total magnitude, scale radius, axis ratio, and position angle, was obtained from the 'photoObj' catalogue using the 'deVMag', 'deVRad', 'deVAB', and 'deVPhi' catalogue parameters, respectively, for each band. These values were used as input in the feedme files to fit a Sérsic profile to the bulge component. In most cases, parameters were left free to vary during fitting to allow convergence on the optimal model. However, in a few instances, parameters were fixed to achieve a stable solution. Given that the initial guesses were close to the expected values, it was assumed that GALFIT would converge with minimal iterations. The Sérsic index was initially set to 1 for all galaxies and allowed to vary during the fitting process. In cases where optical imaging suggested the presence of a disc, an exponential component was included in the model. An initial parameter set for the exponential disc was adopted and used in the fitting process when applicable. The corresponding parameters from the photoObj catalogue 'expMag', 'expRad', 'expAB', and 'expPhi' were provided as inputs in the 'feedme' file. GALFIT was initially executed for all sources to obtain an rms sky estimate, which was subsequently fixed as the sky background value in the corresponding feedme file. Fixing the sky parameter reduced the number of free parameters and, consequently, the number of fitting iterations. In cases with nearby contaminating sources, a custom mask was manually generated and supplied as 'mask.fits'. For some cases, for fitting purposes, an additional Sérsic component was included to model their contribution when there is an extended source nearby.

As the sample consists of merging galaxies, each system contains multiple nuclei, necessitating a multicomponent fitting approach. An initial fit was performed using one Sérsic component per galaxy, each representing a bulge. Thus, every system includes at least two Sérsic components. In cases where the fit was inadequate or a disc was visibly present, an additional exponential component was included to account for the disc. These sources, therefore, include both Sérsic and disc components in the final model.

GALFIT produced satisfactory fits, with acceptable χ^2/ν values, for 69 out of 104 sources (Fig. 1). For the remaining objects, poor residual images indicated model inadequacies. In several cases, GALFIT failed to converge and terminated upon reaching the maximum number of iterations, resulting in no output model. The fitting procedure employed a Sérsic profile for the bulge and an exponential profile for the disc. However, certain disc morphologies exhibited


(a) Image   (b) Model   (c) Residual
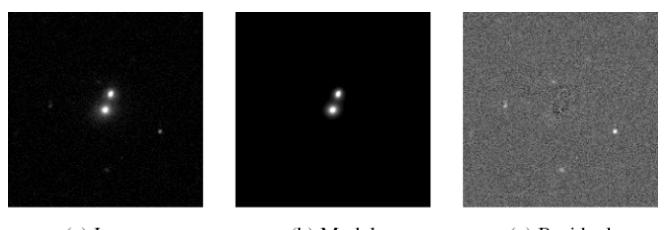
Figure 1. An example to show the result obtained from GALFIT (ObjID: 1237668271362211975).

complex features that this combination could not adequately capture. Several challenges were encountered during the fitting process, leading to the exclusion of a subset of sources from further analysis.

(i) In some cases, GALFIT did not converge owing to insufficient signal-to-noise ratio in one or both galaxies, making extracting reliable structural parameters unfeasible.

(ii) In other cases, the fitting process was not merely affected by contamination from neighbouring sources but failed significantly, resulting in spurious magnitudes and associated parameters. Moreover, systems exhibiting tidal disruption or pronounced morphological disturbances consistently produced unreliable fits, as such features deviate substantially from the assumptions inherent in axisymmetric models.

(iii) For some galaxies, PSF information and initial fitting parameters from SDSS were unavailable, preventing the generation of suitable GALFIT feedme files. Where possible, manual estimates were used in conjunction with available PSFs, but these fits were found to be unreliable and the sources were subsequently excluded.

(iv) Several systems initially appeared as single sources but were classified as multiple components by SDSS, complicating the modelling.

(v) In some cases, closely spaced nuclei led to confusion during fitting, with model functions attempting to fit neighbouring components, resulting in poor residuals.

(vi) Two disc galaxies exhibited intersecting structures and highly diffuse, non-uniform light profiles, which could not be reliably fitted.

After excluding these problematic cases, the sample was reduced from 104 to 69 nuclear pairs used for further analysis. The output of GALFIT is total magnitudes, effective radii, and Sérsic index for the bulge, along with total magnitudes and scale lengths for the disc in each band. The magnitudes in the g and r bands were used to obtain colours for the bulge and disc.

Magnitudes were corrected for Galactic extinction, and K-corrections were also applied to derive the $(g - r)$ colours of bulges in the sample galaxies (D. J. Schlegel, D. P. Finkbeiner & M. Davis 1998; I. V. Chilingarian, A.-L. Melchior & I. Y. Zolotukhin 2010; I. V. Chilingarian & I. Y. Zolotukhin 2012). Five bulges exhibited unphysical negative $(g - r)$ colours, inconsistent with the expected absence of young stellar populations in these systems. These were attributed to fitting errors in the magnitude estimates and were excluded from the analysis. The final sample comprises 64 reliable bulge pairs; this included 61 dual AGN systems and three confirmed triplets (including dual AGN), yielding a total of 131 bulges. The derived colours and applied corrections are listed in Table 1.

For one of the sources in the 61 pairs, there is a third source lying in between (ObjID 1237661812274233474). Although SDSS has classified this source as a GALAXY, there is no spectroscopic data available for the source, and hence no redshift. So we are unable to do further analysis for this source. However, this source had to

Table 1. The colour values as obtained from GALFIT output with further corrections such as extinction correction and *K*-correction. The colour values obtained from these corrected magnitudes and the corresponding stellar mass were calculated using the method mentioned in the text.[a]

ObjID	Band values				Ex corr.				K-corr.				$(g-r)$		Mass ($\times 10^{11}$ M$_\odot$)	
	Bulge		Disc		Bulge		Disc		Bulge		Disc		Bulge	Disc	Bulge	Disc
	g	r	g	r	g	r	g	r	g	r	g	r				
1237650762394959890	16.35	15.36	...	...	16.27	15.31	...	...	16.06	15.23	...	...	0.833	...	4.277	...
1237650762394959891	17.46	16.62	...	...	17.38	16.57	...	...	17.20	16.50	...	...	0.705	...	0.973	...
1237651252018151487	16.75	15.8	...	...	16.62	15.71	...	...	16.43	15.64	...	...	0.794	...	2.355	...
1237651252018151484	16.28	15.26	...	...	16.15	15.17	...	...	15.96	15.10	...	...	0.860	...	4.224	...
1237652600110383328	18.17	17.36	...	...	18.01	17.25	...	...	17.83	17.23	...	...	0.596	...	1.499	...
1237652600110383327	18.81	17.9	...	...	18.65	17.79	...	...	18.38	17.73	...	...	0.653	...	1.383	...
1237653441374453925	20.06	18.54	16.41	15.6	19.96	18.47	16.31	15.53	20.10	18.49	16.16	15.47	1.609	0.688	0.960	1.860
1237653441374453924	17.27	16.37	...	...	17.17	16.30	...	...	17.00	16.24	...	...	0.768	...	1.092	...
1237654382516240489	18.43	17.13	17.49	16.47	18.30	17.04	17.36	16.38	17.91	16.90	17.04	16.27	1.008	0.769	3.601	3.102
1237654382516240490	18.81	17.75	...	...	18.68	17.66	...	...	18.35	17.55	...	...	0.801	...	1.247	...

[a]This is a sample table with limited elements, and the entire table is available in electronic format.
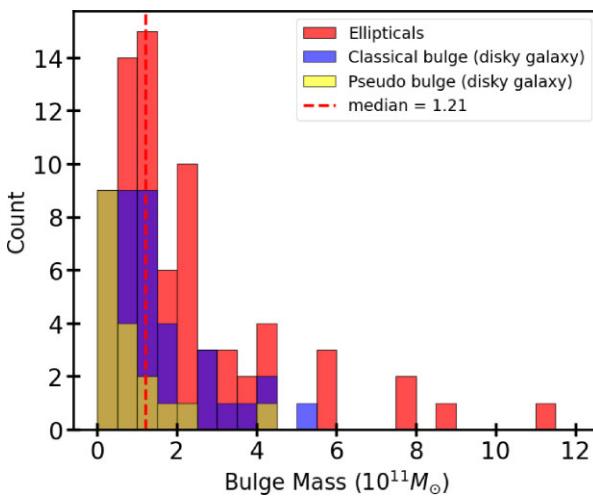
Figure 2. The bulge mass distribution of all the nuclei in the sample. Note that in the sample, 73 were elliptical galaxies and had no disc, whereas 59 were disc galaxies with bulges.
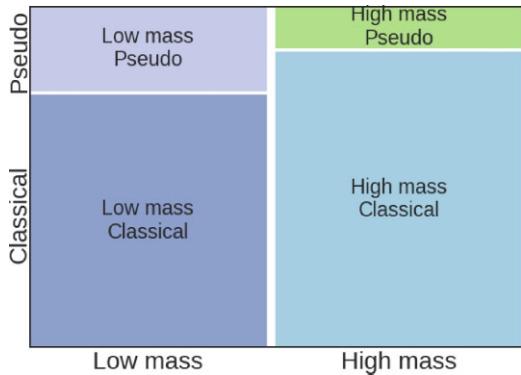

Figure 3. Mosaic of bulge mass and bulge type where bulge mass 1.21×10^{11} M$_\odot$ separates the high- and low-mass bulges.

be fitted in GALFIT in order to fit the neighbouring sources. Hence, Table 1 contains this source with a footnote on why data columns are missing for the source. So the table contains 132 data rows, while our study sample has 131 sources.

3 RESULTS

The $(g - r)$ colour and i-band magnitudes were used to estimate the mass-to-light (M/L) ratio and bulge mass following the prescription of E. F. Bell et al. (2003). The relation

$$\log_{10}(\mathrm{M/L}) = a_\lambda + b_\lambda \times (\mathrm{colour}) \qquad (1)$$

was applied using appropriate coefficients based on the chosen colour and photometric band. The resulting bulge masses are listed in Table 1, and their distribution is shown in Fig. 2. Bulge masses span the range 0.015×10^{11} M$_\odot$ to 1.376×10^{12} M$_\odot$, with the majority falling below 2.5×10^{11} M$_\odot$. One outlier, with $M = 1.10 \times 10^{12}$ M$_\odot$ (ObjID 1237655692474515647), may correspond to an elliptical galaxy rather than a bulge in a disc galaxy; this possibility is discussed further below. A median bulge mass of 1.21×10^{11} M$_\odot$ was adopted to separate the sample into low- and high-mass bulges. A mosaic of this division is presented in Fig. 3.

The distribution of bulge Sérsic indices in the g, r, and i bands is shown in Fig. 4, using uniform bins of width 0.5. The index

ranges and median values are as follows: g band: $0.15 \le n \le 8.56$, median $= 3.13$; r band: $0.33 \le n \le 7.87$, median $= 3.17$; and i band: $0.43 \le n \le 9.95$, median $= 3.27$. Adopting the conventional threshold of $n = 2$ to distinguish classical bulges ($n \ge 2$) from pseudo-bulges ($n < 2$; D. A. Gadotti 2009), we find that 70–80 per cent of bulges in the sample have $n \ge 2$, indicating a predominance of classical bulges. The distributions are similar across all bands, with redder bands tending to yield slightly higher Sérsic indices. This consistency across bands suggests that the prevalence of classical bulges is not an artefact of band-dependent effects. We further examined the relation between bulge type and bulge mass (Fig. 3), which shows that both the most massive bulges and a significant fraction of lower mass bulges exhibit classical bulge nature.

The bulge mass and Sérsic index (n) serve as key morphological indicators. Two galaxy types are distinguished based on GALFIT decomposition:

(i) *Disc galaxies with bulges*. As described in Section 2, if the GALFIT fitting required more than one Sérsic component, the second was consistently modelled as an exponential profile representing a disc. The bulge component is characterized by a Sérsic index n.

(ii) *Elliptical galaxies*. These are well described by a single Sérsic component and lack an associated disc.

Table 2 summarizes the combinations of structural components derived from GALFIT. Among the 131 bulges analysed, 58 are associated with an exponential disc component and are classified as disc galaxies. The remaining 73 lack a disc and are classified as elliptical galaxies. The distribution of bulge and galaxy types is presented in Table 3.

Of the 73 elliptical galaxies ($\sim$64 per cent of the sample), 67 host classical bulges and 6 exhibit pseudo-bulge profiles. These pseudo-bulge ellipticals may retain discy features due to past mergers, or they may be remnants of galaxies that lost their discs through tidal stripping during mergers. Among the 58 disc galaxies, classical bulges dominate, although a substantial number also host pseudo-bulges. Overall, approximately 77 per cent of pseudo-bulges are associated with disc galaxies, while only a small fraction reside in systems without discs.

The pairwise distribution of the Sérsic indices for the 60 merging galaxies is shown in Fig. 5. Triple systems are excluded for clarity, as the focus is on dual AGN systems. The plot is divided into four regions representing different bulge pair types. (i) Classical–classical (C–C) pairs, which include mergers of elliptical galaxies or disc galaxies where both hosts have classical bulges. This region contains the largest number of bulges. (ii) Classical–pseudo (C–P) pairs, spanning two regions, include mergers between a classical and a pseudo-bulge host, either in disc or elliptical galaxies. In most cases, the classical bulge is more massive. (iii) Pseudo–pseudo (P–P) pairs, forming the smallest group, and consist of mergers where both hosts have pseudo-bulges. Major mergers appear scattered across the diagram, while minor mergers are more concentrated in the C–C region. The bulge and host galaxy classifications for each source are listed in Table 2.

One of the key questions addressed in this work is whether dual AGNs are more frequently hosted by mergers of elliptical galaxies, disc galaxies, or mixed pairs. Table 2 summarizes the morphological distribution of dual AGN host galaxies, classified as elliptical–elliptical (E–E), disc–disc (D–D), and elliptical–disc (E–D) mergers. The respective counts are E–E $= 24$, D–D $= 18$, and E–D $= 24$. Two systems are identified as triplets involving D–E–E and D–D–E configurations and are therefore counted twice. Although the sample is neither complete nor statistically unbiased,
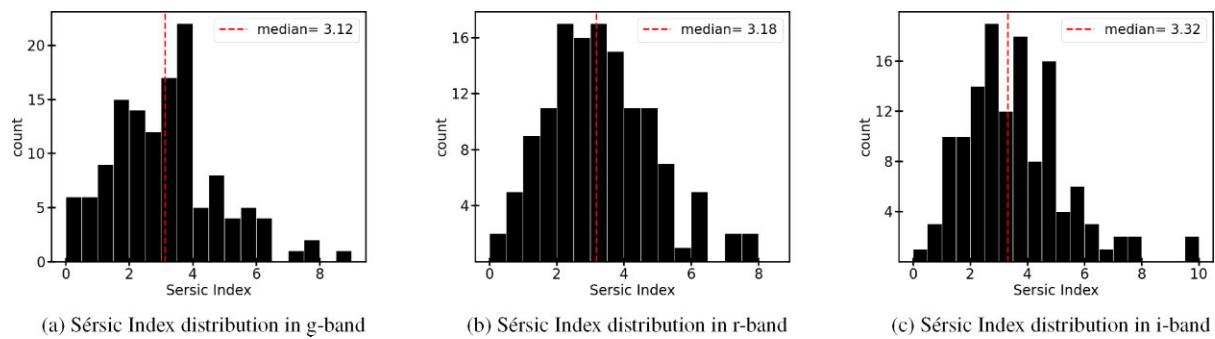
Figure 4. Distribution of Sérsic Index observed over three bands: '*g*', '*r*', and '*i*' from left to right.

Table 2. A table representing the merging galaxy pairs. The combinations are galaxy type (ellipticals or discy), bulge type (classical or pseudo), and mass ratio (major merger if mass ratios < 3, minor merger for values > 3).[a]

No.	ObjID	Exp disc	Disc combination	Sersic index	Bulge type	Bulge pair	Stellar mass	Mass ratio
1	1237650762394959890	No	Elip–Elip	5.87	Classical	C–C	4.277	4.396
1	1237650762394959891	No		5.5	Classical		0.973	
2	1237651252018151487	No	Elip–Elip	5.55	Classical	C–C	2.355	1.793
2	1237651252018151484	No		4.48	Classical		4.224	
3	1237652600110383328	No	Elip–Elip	4.58	Classical	C–P	1.499	1.084
3	1237652600110383327	No		0.98	Pseudo		1.383	
4	1237653441374453925	Yes	Disc–Elip	1.03	Pseudo	C–P	2.820	2.582
4	1237653441374453924	No		3.76	Classical		1.092	
5	1237654382516240489	Yes	Disc–Elip	4.14	Classical	C–C	6.702	5.377
5	1237654382516240490	No		7.79	Classical		1.247	

[a]This is a sample table with limited elements, and the entire table is available in electronic format.

Table 3. Bulge type versus disc presence.

	Classical bulge	Pseudo-bulge	Total
No disc	67	6	73
With disc	38	20	58
Total	105	26	131

the results suggest that dual AGNs are more commonly associated with elliptical (E–E) and mixed (E–D) mergers than with disc–disc (D–D) systems. This is consistent with the expectation that dual AGNs are associated with galaxies that have undergone mergers, since elliptical galaxies preferentially reside in denser environments relative to disc galaxies (A. Dressler 1980). A similar trend is evident in the colour–magnitude plot of the GOTHIC sample (A. Bhattacharya et al. 2023), where dual AGNs predominantly occupy the red, evolved galaxy population in the plot.

Using GALFIT-derived scale radii, the bulge sizes of the 131 nuclei are compared. For disc galaxies, this corresponds to the bulge effective radius (R_e), while for ellipticals it represents the overall galaxy scale radius. Fig. 7(a) shows that ellipticals exhibit R_e values extending up to 21 kpc, whereas disc galaxies have $R_e < 6$ kpc, which may correspond to a bar embedded within a faint disc or a discy elliptical galaxy. Overall, the plot highlights a clear dichotomy between the scale lengths of discs and those of elliptical galaxies.

In this study, we consider mergers with galaxy mass ratios ≤ 3 to be major mergers and those with mass ratios > 3 as minor mergers. This threshold was chosen as a value close to the 1:1 ratio would be more accurate as a major merger candidate and is also consistent with the numerical studies on mergers in the nearby universe (C. J. Conselice 2006). Fig. 7(b) shows the distribution of major mergers and minor mergers. One source appears to have a very large mass

ratio (ObsID 1237655502962688659). For this source, one galaxy appears to be embedded inside the disc of the companion galaxy, which appears to be relatively large. But overall our results indicate that ∼60 per cent of dual AGNs are associated with major mergers. If we assume major mergers to have galaxy mass ratios ≤ 4, then the fraction of dual AGNs in major mergers become even larger.

Finally, the bulge-to-total stellar mass ratio (B/T) was estimated for the sample of 58 disc galaxies. The distribution of B/T values, along with the bulge-to-disc ratio (B/D) as a function of total stellar mass, is presented in Fig. 7(c). The B/T values range from ∼0.1 to 0.95. Systems with B/T > 0.6 are bulge dominated, exhibiting faint stellar discs. Such galaxies may correspond to S0 types or giant low surface brightness (GLSB) galaxies, both known to host diffuse stellar discs. As GLSB galaxies are typically isolated, the high B/T values are likely associated with S0 galaxies in the sample.

4 DISCUSSION

The structural and morphological analysis of dual AGN host galaxies offers important insights into the conditions conducive to forming and detecting SMBH pairs. Our results reveal a strong preference for dual AGN to reside in systems with classical bulges, typically characterized by high Sérsic indices ($n > 2$) and elevated bulge masses. This preference is closely tied to the evolutionary history of their host galaxies, with major mergers playing a central role in shaping the stellar and dynamical environments favourable for dual AGN activity. In the following paragraphs, we examine the key trends emerging from our study and place them in the broader context of AGN triggering mechanisms and SMBH binary formation.

Our structural analysis reveals that dual AGNs are predominantly hosted by galaxies with Sérsic indices $n > 2$, indicating the presence

(a) Combination of Sérsic index in g-band   (b) Combination of Sérsic index in r-band   (c) Combination of Sérsic index in i-band
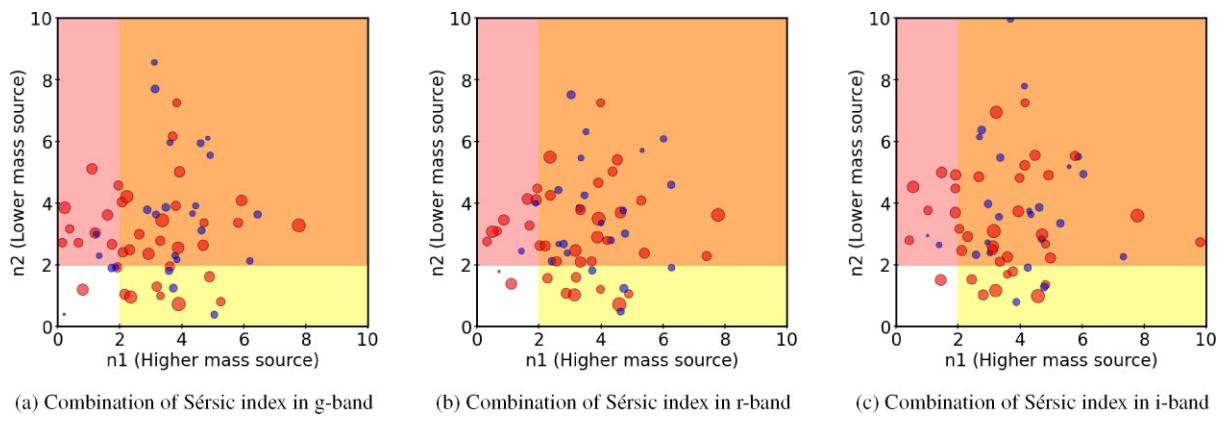
Figure 5. The three plots from left to right show, respectively, the pairing of Sérsic index in merging samples, where n_1 and n_2 correspond to the Sérsic index of the heavier and lighter bulge mass nuclei, respectively. The size of the scatter points depends inversely on the bulge mass ratio, where a lower bulge mass ratio ($1 < M_1/M_2 < 3$), which is the major merger sample, is indicated in red, and the higher bulge mass ratio ($M_1/M_2 \geq 3$), which is the minor merger sample, is represented as blue.
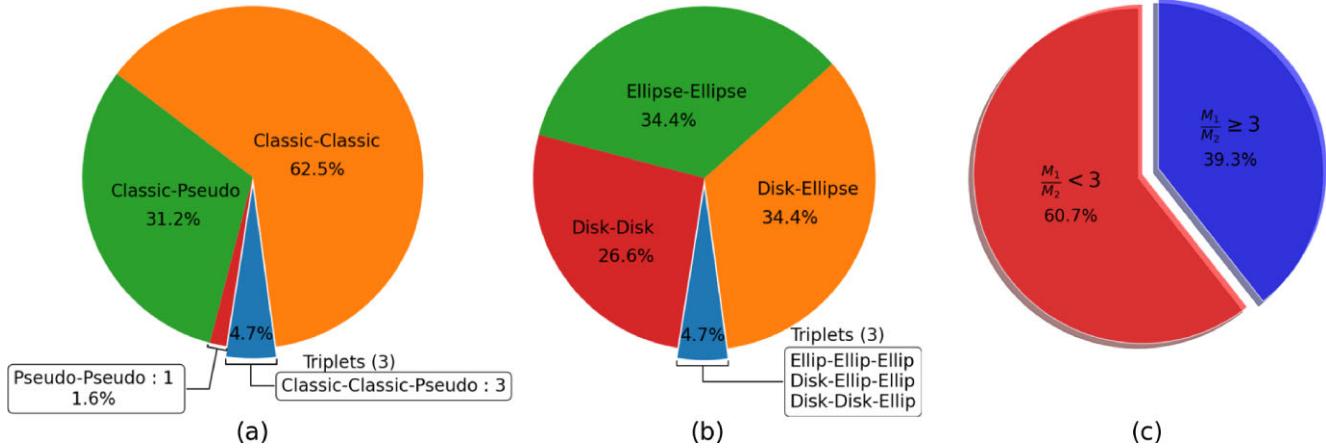
Figure 6. Pie diagrams from left to right. (a) The extreme left shows the different types of bulge combinations. (b) The centre shows the fraction of different merger types. (c) The extreme right shows the major versus minor merger numbers.
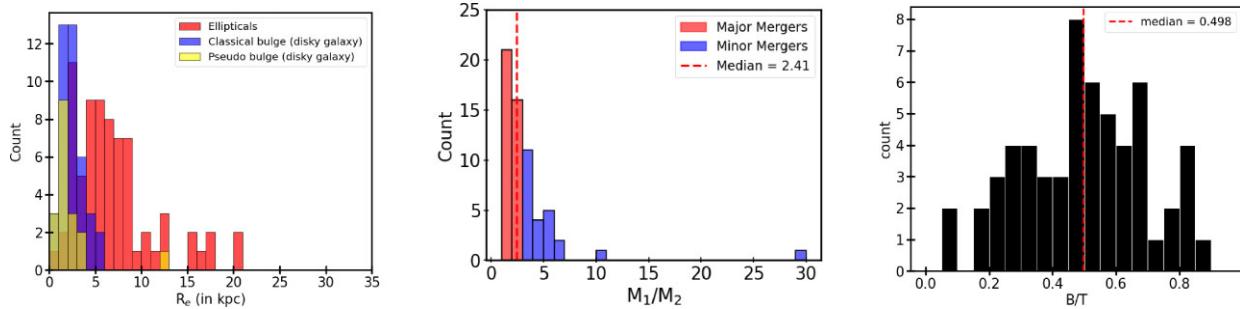
Figure 7. From left to right. (a) The distribution of bulge scale radius R_e in disc galaxies or the galaxy scale radii of elliptical galaxies. (b) The distribution of total galaxy mass ratios for the sample. Note that there are two outliers having mass ratios ~ 10 and ~ 30. (c) The ratio of bulge to total galaxy mass for the 58 disc galaxies in our sample, where the median value is shown with a dashed vertical line.

of classical bulges that are typically found in elliptical or bulge-dominated disc galaxies. As shown in Fig. 4, the median Sérsic index across all wavebands exceeds 2. So classical bulges are notably prevalent among dual AGN host galaxies. Classical bulges also exhibit higher bulge masses (Figs 2 and 3). Assuming that the established $M-\sigma$ relation observed in AGN host galaxies is valid for the bulges of dual AGNs (N. J. McConnell & C.-P. Ma 2013),

our results suggest that the merging process leads to the growth of SMBHs as well. It also suggests that SMBH binaries preferentially reside in merger remnants with $n > 2$.

Dual AGNs are also more commonly found in elliptical pairs or elliptical–disc pairs. Based on Sérsic model fits, systems with a single high-Sérsic component are classified as ellipticals, while those with two components are identified as bulge–disc systems. Assuming

this classification, approximately two-thirds of the sample contain classical bulges in both galaxies (Fig. 6). Also, 94 per cent of dual AGNs host at least one such bulge (Figs 5 and 6). As mentioned earlier, classical bulges are generally formed from the monolithic collapse of galaxies at early epochs or via the major mergers of galaxies. They are characterized by redder, older stellar populations, in contrast to pseudo-bulges that are formed via secular processes and are relatively bluer in colour (J. Hu et al. 2024b). This trend is consistent with previous findings (A. Bhattacharya et al. 2023), which show that dual AGNs preferentially occupy the red sequence in colour–magnitude space.

Pseudo-bulges are rare among dual AGN hosts, and systems comprising two pseudo-bulges are exceptionally uncommon (Fig. 6). This further reinforces the link between classical bulge formation via mergers and the occurrence of dual AGNs, as opposed to dual AGNs in pseudo-bulges formed through secular evolution.

Finally, dual AGNs are predominantly associated with major mergers, with typical stellar mass ratios ≤ 3, as seen in the final panel of Fig. 6. This result is consistent with earlier observational studies (A. Stemo et al. 2021) and suggests that major mergers play a key role not only in AGNs triggering but also in the formation of SMBH binaries. These findings have important implications for the identification and characterization of SMBH binaries in forthcoming low-redshift surveys.

5 CONCLUSIONS

In this study, we investigate the structural properties, host galaxy morphologies, and bulge classifications of dual AGN systems in the GOTHIC sample, based on two-dimensional decompositions of SDSS imaging. Our main results are as follows:

(i) The bulge masses of dual AGN host galaxies span 1.5×10^9 M to 1.4×10^{12} M$_\odot$, with the most massive bulges corresponding to elliptical galaxies.

(ii) Sérsic indices in the *g*, *r*, and *i* bands indicate that 80 per cent (105/131) of bulges are classical. Of these, 64 per cent (67) are found in elliptical galaxies, while 36 per cent (38) reside in disc galaxies. The remaining 20 per cent (26) are pseudo-bulges with significant discy components.

(iii) Host morphologies reveal that dual AGNs are more frequently found in elliptical–elliptical (E–E) and elliptical–disc (E–D) mergers than in disc–disc (D–D) mergers. Approximately two-thirds of the systems include at least one elliptical galaxy, while only 30 per cent involve two disc galaxies. This suggests a preference for red, evolved hosts over star-forming systems.

(iv) Nearly 60 per cent of dual AGNs are associated with major mergers. Combined with their prevalence in red, quiescent galaxies, this supports the interpretation that dual AGNs predominantly reside in quenched environments with low star formation activity.

These findings suggest that dual AGNs predominantly arise from major mergers and are preferentially hosted by massive, evolved systems – either classical bulges in discs or elliptical galaxies – consistent with merger-driven evolutionary pathways.

ACKNOWLEDGEMENTS

DATA AVAILABILITY

This article has made use of SDSS DR18 data, which is public data and available online.

REFERENCES

Abbott B. P. et al., 2016, Phys. Rev. Lett., 116, 061102
Bailes M. et al., 2021, Nat. Rev. Phys., 3, 344
Baldwin J. A., Phillips M. M., Terlevich R., 1981, PASP, 93, 5
Bell E. F., McIntosh D. H., Katz N., Weinberg M. D., 2003, ApJS, 149, 289
Bhattacharya A., Nehal C. P., Das M., Paswan A., Saha S., Combes F., 2023, MNRAS, 524, 4482
Bridge C. R., Carlberg R. G., Sullivan M., 2010, ApJ, 709, 1067
Brooks A., Christensen C., 2016, in Laurikainen E., Peletier R., Gadotti D., eds, Galactic Bulges. Springer, Cham, Switzerland, p. 317
Burke-Spolaor S. et al., 2019, A&AR, 27, 5
Byrd G., Valtonen M., 2001, AJ, 121, 2943
Chilingarian I. V., Zolotukhin I. Y., 2012, MNRAS, 419, 1727
Chilingarian I. V., Melchior A.-L., Zolotukhin I. Y., 2010, MNRAS, 405, 1409
Conselice C. J., 2006, ApJ, 638, 686
Cox T. J., Primack J., Jonsson P., Somerville R. S., 2004, ApJ, 607, L87
Cox T. J., Jonsson P., Somerville R. S., Primack J. R., Dekel A., 2008, MNRAS, 384, 386
Das M., Rubinur K., Kharb P., Varghese A., Novakkuni N., James A., 2018, Bull. Soc. R. Sci. Liege, 87, 299
Debattista V. P., Carollo C. M., Mayer L., Moore B., 2004, ApJ, 604, L93
De Rosa A. et al., 2019, New Astron. Rev., 86, 101525
Dressler A., 1980, ApJ, 236, 351
Eggen O. J., Lynden-Bell D., Sandage A. R., 1962, ApJ, 136, 748
Fisher D. B., Drory N., 2016, in Laurikainen E., Peletier R., Gadotti D., eds, Galactic Bulges. Springer, Cham, Switzerland, p. 41
Gadotti D. A., 2009, MNRAS, 393, 1531
Ghosh S., Fragkoudi F., Di Matteo P., Saha K., 2024, A&A, 683, A196
Giri G., Dubey R. P., Rubinur K., Vaidya B., Kharb P., 2022, MNRAS, 514, 5625
Graham A. W., Driver S. P., 2005, Publ. Astron. Soc. Aust., 22, 118
Hopkins P. F., Hernquist L., Cox T. J., Keres D., Wuyts S., 2009, ApJ, 691, 1424
Hopkins P. F. et al., 2010, ApJ, 715, 202
Hu J., Wang L., Ge J., Zhu K., Zeng G., 2024a, MNRAS, 529, 4565

Hu J., Cui Q., Wang L., Pei W., Ge J., 2024b, A&A, 691, A125

Keshri S., Barway S., Das M., Yadav J., Combes F., 2025, A&A, 695, A39

Kharb P., Lal D. V., Merritt D., 2017, Nat. Astron., 1, 727

Komossa S., Burwitz V., Hasinger G., Predehl P., Kaastra J. S., Ikebe Y., 2003, ApJ, 582, L15

Kormendy J., Fisher D. B., 2008, in Funes J. G., Corsini E. M., eds, ASP Conf. Ser. Vol. 396, Formation and Evolution of Galaxy Disks. Astron. Soc. Pac., San Francisco, p. 297

Kormendy J., Kennicutt R. C., Jr, 2004, ARA&A, 42, 603

Koss M., Mushotzky R., Treister E., Veilleux S., Vasudevan R., Trippe M., 2012, ApJ, 746, L22

Kumar A., Kataria S. K., 2022, MNRAS, 514, 2497

Kumar A., Das M., Kataria S. K., 2021, MNRAS, 506, 98

Li F., Rahman M., Murray N., Kereš D., Wetzel A., Faucher-Giguère C.-A., Hopkins P. F., Moreno J., 2025, ApJ, 979, 7

McConnell N. J., Ma C.-P., 2013, ApJ, 764, 184

Marsden C., Shankar F., Ginolfi M., Zubovas K., 2020, Front. Phys., 8, 61

Méndez-Abreu J., Debattista V. P., Corsini E. M., Aguerri J. A. L., 2014, A&A, 572, A25

Mihos J. C., Hernquist L., 1996, ApJ, 464, 641

Mondal S., Das M., Rubinur K., Bansal K., Nath A., Taylor G. B., 2024, A&A, 691, A279

Nandi S., Das M., Dwarakanath K. S., 2021, MNRAS, 503, 5746

Padmanabhan H., Loeb A., 2024, A&A, 684, L15

Peng C. Y., Ho L. C., Impey C. D., Rix H.-W., 2002, AJ, 124, 266

Pfeifle R. W. et al., 2019, ApJ, 883, 167

Quilley L., de Lapparent V., 2022, A&A, 666, A170

Rubinur K., Das M., Kharb P., 2018, J. Astrophys. Astron., 39, 8

Rubinur K., Das M., Kharb P., 2019, MNRAS, 484, 4933

Rubinur K., Kharb P., Das M., Rahna P. T., Honey M., Paswan A., Vaddi S., Murthy J., 2021, MNRAS, 500, 3908

Sachdeva S., Saha K., Singh H. P., 2017, ApJ, 840, 79

Schechter A. L. et al., 2025, ApJ, 989, 149

Schlegel D. J., Finkbeiner D. P., Davis M., 1998, ApJ, 500, 2

Stemo A., Comerford J. M., Barrows R. S., Stern D., Assef R. J., Griffith R. L., Schechter A., 2021, ApJ, 923, 36

Vaghmare K., Barway S., Kembhavi A., 2013, ApJ, 767, L33

Valtonen M. J. et al., 2022, MNRAS, 514, 3017

Valtonen M. J. et al., 2025, ApJ, 992, 110

White S. D., Frenk C. S., 1991, ApJ, 379, 52

Yadav J., Das M., Barway S., Combes F., 2021, A&A, 651, L9

Zavala J., Avila-Reese V., Firmani C., Boylan-Kolchin M., 2012, MNRAS, 427, 1503

Zhang Y.-W., Huang Y., Bai J.-M., Liu X.-W., Wang J.-g., Dong X.-b., 2021, AJ, 162, 276

SUPPORTING INFORMATION

Supplementary data are available at *MNRAS* online.

table1
table2

Please note: Oxford University Press is not responsible for the content or functionality of any supporting materials supplied by the authors. Any queries (other than missing material) should be directed to the corresponding author for the article.

This paper has been typeset from a TEX/LATEX file prepared by the author.